communications biology

Article

https://doi.org/10.1038/s42003-024-07289-w

Single-cell immune profiling and validation of PBMCs in the onset of and recovery from herpes zoster

Shang Zheng[1,3], Shuyao Zhang[1,3], Xiangyao Li[2], Yong Fei[1], Lei Yang[1], Beibei Liu[1], Kangli Shen[1], Qinli Feng[1], Qinghe Zhou[1], Ming Yao[1] ✉ & Longsheng Xu[1] ✉

To gain deeper insights into pathogenesis of herpes zoster, the peripheral blood mononuclear cells (PBMCs) from male patients mostly were subjected to single-cell RNA-seq (scRNA-seq) and ATAC-seq analysis. Here we show a detailed immune cell profile in the onset of and recovery from herpes zoster, revealing proportion alterations of the subpopulations, which were validated by flow cytometric analysis and comparison of blood routine data. The integrative analysis of the transcriptomes and epigenomes provided a comprehensive description and validation of the key changes in peripheral blood. This study may provide deep insight into the immune profile during herpes zoster progression and holds potential clinical significance.

Herpes zoster, a viral syndrome caused by the reactivation of varicella-zoster virus (VZV), affects approximately thirty percent of the global population[1–3]. The rash typically resolves within 2 to 3 weeks, but postherpetic neuralgia (PHN), a common complication of herpes zoster can last for an extended period[4]. Antiviral medications as the primary treatment option can only help shorten the duration of the rash but do not prevent PHN[5].

Varicella-zoster virus is one of the five human herpes viruses, which also includes herpes simplex virus 1 and 2 (HSV-1, HSV-2), cytomegalovirus and Epstein-Barr virus[6]. Varicella (chicken pox) is a primary infection of VZV that causes ganglionic latency in neurons, usually in children[7]. Latency occurs in ganglia across the neuroaxis, encompassing the dorsal root ganglia (DRG), trigeminal ganglia (TG), as well as autonomic ganglia, including the enteric ganglia. Reactivation of localized reactivation of the VZV causes herpes zoster, which usually occur in adults. And the susceptibility to herpes zoster is increased in elderly people as well as immune compromised population[8]. In addition, post-herpetic neuralgia (PHN), a condition notably resistant to treatment, represents the most recognized complication of herpes zoster. It is characterized by severe and persistent pain in the affected dermatome, persisting for more than three months following the resolution of the zoster rash[9]. Moreover, studies revealed that the natural history of herpes zoster is significantly affected by the host's immune status[10–12]. Vaccines are currently the only effective means of preventing shingles and neuralgia, and are 90% effective in adults with healthy immune systems[13]. However, vaccines are a means of prevention not a cure still with possible side effects. Mechanisms and cure of herpes zoster and postherpetic neuralgia still urgently need to be explored.

Previous study reported the number of CD3+ T-lymphocytes and CD8+ T-lymphocytes were decreased in patients with herpes zoster[14]. Furthermore, several types of innate cells have been reported to play a role in the initial immune defense against herpes zoster, such as natural killer cells, monocytes as well as neutrophils[15–19]. In view of the above correlation between immune cells and clinical features of herpes zoster. The present study utilized scRNA-seq and ATAC-seq methods to analyze the PBMCs from different herpes zoster stages. Our analysis provided a detailed immune cell profiling of peripheral blood cells in the herpes zoster-onset stage, revealing an elevated proportion of T, MPs and B cells in HP, while the proportion of neutrophils was significantly downregulated. These findings also showed specific increases in the expression of inflammatory genes and OCRs in the inflammatory and transcriptional control regions. In addition, the epigenomics analysis highlighted the t cell and neutrophil activation in HP at bulk level. Significant alterations were noted in T cells, particularly in CD8+ Teff cells, characterized by subtype alteration and functional shift. Metabolic activities and the cytokine-related pathways were revealed to be enriched in neutrophil subpopulations. It demonstrated that the proportion of monocytes, especially CD14+ classical monocytes, was increased in HP, and further analysis revealed that inflammatory gene expression such as Il-1b was activated in monocytes. In addition, the memory B cell and plasma cells were upregulated in B cell cluster, and the enrichment analysis of the two subpopulations suggested the maturation and activation of B cells in HP group. Distinct from previous studies, the present study holds potential clinical significance as it provides a comprehensive description and validation of the key changes in peripheral blood.

[1]Department of Anesthesia and Pain Medicine, Affiliated Hospital of Jiaxing University, Jiaxing, 314000, China. [2]The Fourth Affiliated Hospital, Zhejiang University School of Medicine, Yiwu, 322000, China. [3]These authors contributed equally: Shang Zheng, Shuyao Zhang. ✉e-mail: jxyaoming@zjxu.edu.cn; xlsh2468@zjxu.edu.cn

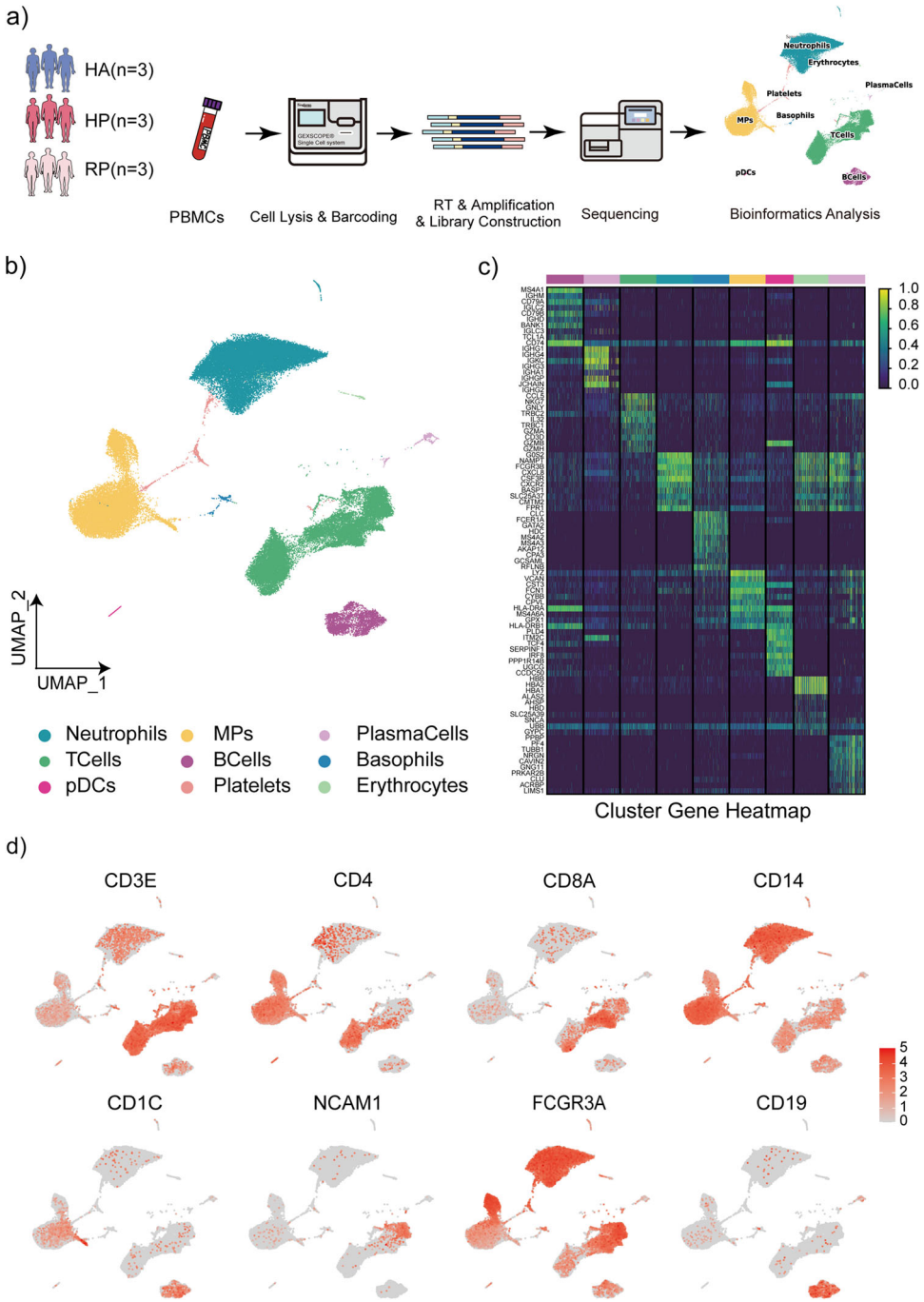

Fig. 1 | Study design and analysis of single immune cell profiling in the onset of and recovery from herpes zoster. a Schematics of the experimental design for single-cell RNA (sc-RNA) sequencing. Peripheral blood mononuclear cells (PBMCs) were processed via sc-RNA sequencing using the 10x-Based Genomics platform after collected from herpes zoster patients (HP), herpes zoster patients after recovery (RP) and healthy controls (HA). **b** UMAP plot showing eight subpopulations of PBMCs including neutrophils, MPs, plasma cells, T cells, B cells, basophils, CDCs, platelets and erythrocytes identified using integrated and classification analysis. **c** The heatmaps show differentially expressed genes (DEGs) upregulated in eight subpopulations of PBMCs. **d** UMAP projection of canonical markers, including CD3E, CD4, CD8A, and NCAM1 for NK and T cells; CD14, CD1C, and FCGR3A for myeloid cells; and CD19 for B cells as indicated in the legend.

Results

Single- cell profiling and cell type identification of PBMCs in simple herpes virus patients

To map the immune microenvironment of herpes zoster patients, we identified changes in the blood and pinpointed cell-specific alterations associated with disease severity and recovery, single-cell RNA sequencing (scRNA-seq) was conducted on peripheral blood mononuclear cells (PBMCs) obtained from three groups: three samples were collected from patients with herpes zoster as HP group, three samples were collected from patients recovered from herpes zoster as RP group, and three samples were collected from healthy individuals as HA group (Fig. 1a and Supplementary Fig. 1). Two samples in the HP group and Two samples in the RP group were from the same individual separately to minimize the effect of individual differences in this study.

Following quality control measures, a total of 66,338 cells from the mentioned groups were subjected to analysis. This dataset passed stringent high-quality filtering. Single-cell suspensions of the scRNA-seq samples were converted to barcoded scRNA-seq libraries using 10× Genomics. Cell Ranger software (version 3.1.0) was used for the initial processing of the sequencing data. Subsequently, single-cell sequencing data were analyzed to discover more about the immunological profile of herpes zoster. Using Uniform Manifold Approximation and Projection (UMAP), we analyzed the distribution of the three immune cell lineages: myeloid, NK and T, as well as B cells, based on the expression of canonical lineage markers and other genes specifically upregulated in each cluster (Fig. 1b, c). For marker genes, expression values in each cell positioned in a UMAP are shown in Fig. 1d. We next clustered the cells of each lineage separately and identified a total of 20 immune cell clusters.

An overview of immune cells in the blood of herpes zoster patients

Altogether, 3587 B cells, 780 plasma cells and 19,745 T cells, and 25,859 neutrophils, 305 Basophils, 6330 MPs, and 230 pDCs were included in the scRNA-seq profile. The merged image of each group is shown in Fig. 2a. We discovered that both the HP and RP group demonstrated a higher proportion of T cells and MPs compared to the HA group, but with a lower proportion of B cells, neutrophils, erythrocytes and platelets (Fig. 2b). Additionally, the proportion of B cells, especially plasma cells, was lower in the HP group compared to RP group. Interestingly, the HP group had more B cells, NK cells, and T cells, but fewer myeloid cells than the RP group (Fig. 2b).

To further understand the changes in the myeloid, NK and T, and B cells in herpes zoster patients, we conducted differential expression gene (DEG) analysis of the NK, T, B, neutrophils and myeloid cells among the three groups (Fig. 2c–f). We found that in the two patient groups, the inflammatory genes including *IL-1b, TNF, JUNB* and *CXCL10* as well as cytokines were highly expressed in the NK, T, B, neutrophils and myeloid cells.

We also investigated the routine blood data of 1000 patients with herpes zoster, and the proportion of peripheral blood cells accounted for by monocytes was upregulated, consistent with the results of single-cell sequencing, while the overall difference in the proportion of lymphocytes was not significant, a small number of patients exhibited significantly higher proportions of lymphocytes compared to the controls (Fig. 2g–j). We also collected clinical samples of neutrophils and B cells, and our analysis indicated a consistent tendency with scRNA-seq (Supplementary Fig. 2).

Collectively, our results demonstrated that myeloid cells and neutrophils decreased, whereas NK and T cells increased in the peripheral blood of herpes zoster patients and that the immune cell compositions differed between the patients in the HP group and RP group.

Integrated analysis of bulk DAR and bulk DEG revealed the transcriptomic and epigenetic differences between PBMCs in HA and HP

An integrated analysis of DEGs and DARs at bulk levels (bulk-DEGs and bulk-DAR) was performed to determine the transcriptomic and epigenetic differences between PBMCs in HA and HP group (Fig. 3a). A gene-OCR pair was based on the identification of an OCR that regulated the expression of a specific gene (Fig. 3b). The results of ATAC-seq analyses are shown in the genome browser for OCRs corresponding to key genes enriched in scRNA-seq analysis between HA and HP (Fig. 3c). The ATAC-seq analysis found that the chromatin regions in *ITGAM, IFNG, TLR1, IRF1* were more open in HP than in HA among the more accessible OCRs in HP than HA. Furthermore, it was revealed that expression of the genes mentioned above were also higher in HP according to scRNA-seq (Fig. 3c). Motif analysis of the DARs identified transcription factors (TFs) enriched in HP group The top 8 motifs motif analysis of the up-regulated Peaks and the predicted motif-related key transcription factors were ZF family, such as *CTCF* motif and *BORIS* motif, and *ETS* family, such as *Elf4* motif and *ETS1* motif (Fig. 3d).

In addition, the GO enrichment analysis for bulk-DARs showed that T cell activation, lymphocyte differentiation, alpha-beta T cell activation, T cell differentiation, cellular response to peptide and neutrophil activation were highly enriched in HP (Fig. 3e). KEGG pathway enrichment analysis was to determine enriched pathways of predicted TFs, ranking high on this list of pathways enriched in HP were neutrophil activation, neutrophil degranulation, neutrophil activation involved in immune response, neutrophil mediated immunity, leukocyte differentiation, T cell activation. And the most enriched pathways in HA were response to endoplasmic reticulum stress, positive regulation of mRNA metabolic process, response to topologically incorrect protein, mRNA catabolic process, RNA catabolic process, RNA splicing, and proteasomal protein catabolic process.

The distribution of NK and T cell characterized by single-cell sequencing

NK and T cells comprised 19,718 cells, which allowed us to deeply interrogate subpopulation structures and disease progression-dependent changes within these subpopulations (Fig. 4a). Our analysis divided NK and T cells into 7 clusters based on the classical markers: *CD8A, CD4, CCR7, GZMK, NCAM1, GNLY, FCGR3A, MKI67, FOXP3* (Fig. 4b). NK cells highly expressed *GNLY, FCER1G* and *TYROBP*. CD8+ T cells expressed *CD8A* and *CD8B* and were sub-divided into three clusters: naïve CD8+ T cells, which expressed high levels of *CCR7, LEF1*, and *TCF7*, similar to naïve CD4+ T cells; cytotoxic CD8+ lymphocytes (CD8+ CTL), which expressed high levels of *GZMB, GNLY*, and *PRF1*; proliferating T cells were *TYMS*+*MKI67*+ cells and effector memory CD8+ T cells. CD4+ T cells expressed *CD3E* and *CD4*; then, we sub-divided these cells into four clusters: naïve CD4+ T cells (T1), which expressed high levels of *CCR7, LEF1*, and *TCF7*; and regulatory T cells (T4, Treg), which expressed *FOXP3*. The CD4+ T cell subpopulations expression was demonstrated in UMAP plots (Supplementary Fig. 3a).

The compartment of the T cell subpopulations differed remarkably between patients and the HA group (Fig. 4c, d). Proliferating T cell was accumulated in HP group, and CD8+ Teff cells was decreased in HP group without reaching statistical significance. To validate our findings, we devised a flow cytometry panel (Supplementary Table 2) guided by the results from scRNA-seq. We analyzed PBMCs from 39 individuals (20 healthy vs. 19 patients, see Fig. 5a; Supplementary Table 4) focusing on subpopulations emerging from our scRNA-seq analysis. Consistent with scRNA-seq data, we observed that CD4+ T cells did not change, and CD8+ T cells were decreased during the infection. We further performed receiver-operating characteristic (ROC) curve analysis between the HA and HP group to evaluate the diagnostic value of this subset for herpes zoster. ROC curve analysis indicated that distinctive changes occurred with herpes zoster in CD3+ T and CD8+ T cell subset, with the area under curve being 0.93 (Fig. 5d), 0.96 (Fig. 5e). Thus, through scRNA-seq and flow cytometry, we confirmed that CD8+ T cells are useful for distinguishing the HP group from the HA group.

The upregulated genes in CD8 Teff cells of HP group were inflammation-associated genes, and the GO enrichment analysis revealed that T cell activation, response to virus, T cell receptor signaling pathway, IL-12 mediated signaling pathway and response to TNF were enriched in the CD8Teff subpopulation of HP group compared to the HA group (Fig. 5f, g). Enrichment in KEGG indicated that Toll like receptor signaling pathway and MAPK signaling pathways were highly elevated in the HP group (Fig. 5h, i). We looked into the enrichment analysis in RP group than HP group, it was noted that the pathways elevated in HP group compared with HA group was down-regulated in RP group than HP group, indicating that the pathways mentioned above functioned during the progression of herpes zoster (Supplementary Fig. 3b–d). Meanwhile, the functional changes in CD8 Tem subpopulation revealed that response to virus, T cell activation, cellular response to interferon-gamma were stimulated in HP group and maintained in CD8 Tem cells after recovery (Supplementary Fig. 3e–i).

We used CellphoneDB to map the average gene expression of each cell type to known ligand-receptor interactions in order to study the association between T cell clusters and other cell subtypes and demonstrated the top30 ligand–receptor interactions. We first demonstrated that T cells presented a stronger association with neutrophils through RPS19_C5AR1 (Fig. 5j). A previous study identified that the interaction between them can regulate the migration and apoptosis of neutrophils[20]. Using Monocle 2, cells were ordered in a pseudotime manner to investigate the molecular mechanisms that govern the development of T cells during disease progression. Three states were identified by pseudotime trajectory analysis, accompanied by pseudotime flows and distributions of cell states (Fig. 5k–m). Our unsupervised trajectory analysis by Monocle2 showed that Naïve T cells and GDT cells were at the root of the trajectory, Treg cells was located in the middle of the trajectory, while NK cell CD8+ T cells and Proliferating T cells were found in all branches.

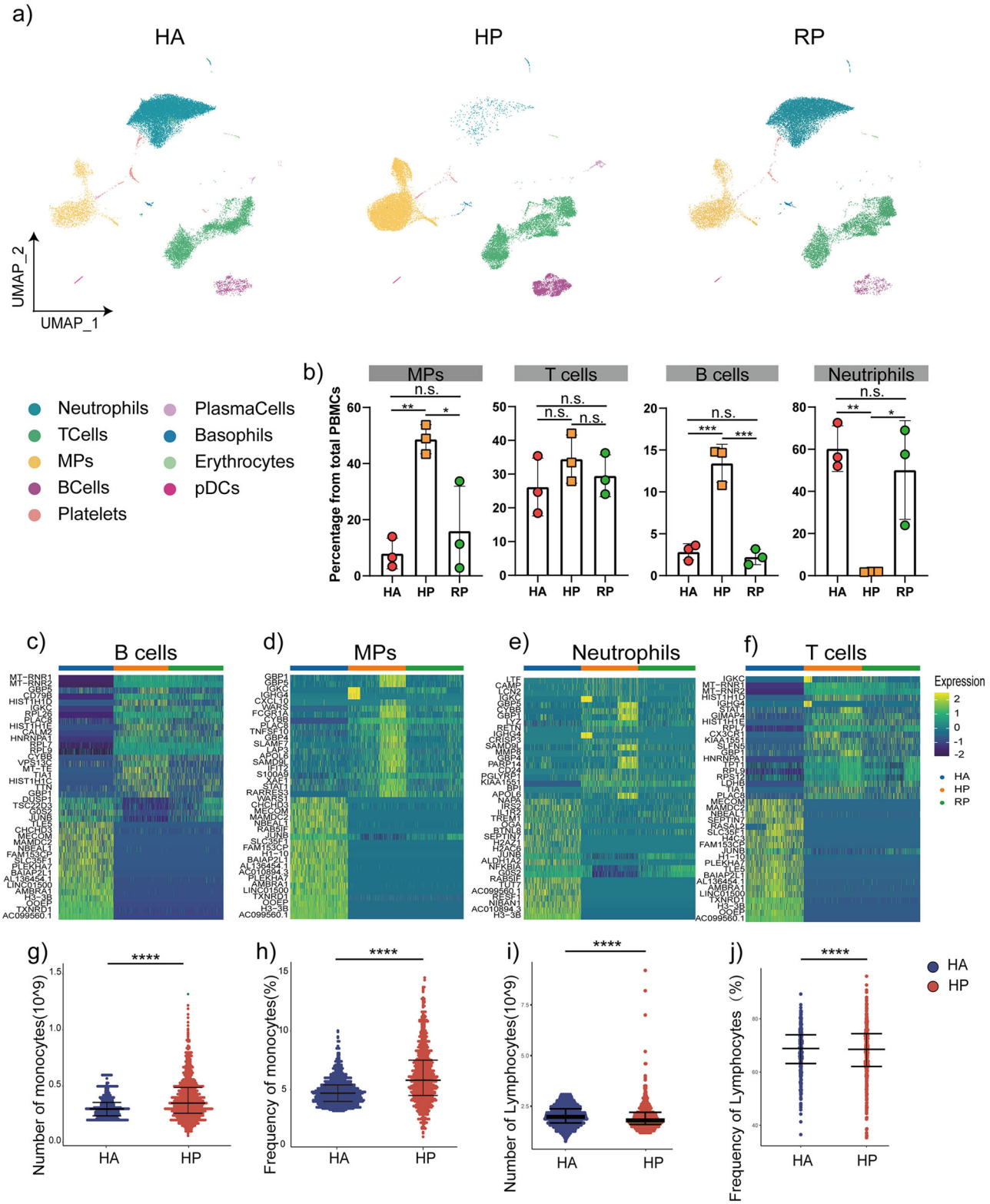

Fig. 2 | An overview of NK and T, B, and myeloid cells in the blood of three groups. a The UMAP plot shows a comparison of the clustering distribution across HCs as well as herpes zoster patients (HP) and herpes zoster patients (RP) patients. **b** The bar plot shows the relative contributions of eight subpopulations by samples, including three HAs, three HP patients, and three RP patients. **c** The box diagram shows the percentages of myeloid, NK and T, and B cells across the three groups. **d** The heatmap shows the DEGs of B cells among the HAs, herpes zoster patients (HP) and herpes zoster patients (RP) patients. **e** The heatmap shows the DEGs of MPs among the HAs, herpes zoster patients (HP) and herpes zoster patients (RP) patients. **f** The heatmap shows the DEGs of neutrophils among the HAs, herpes zoster patients (HP) and herpes zoster patients (RP) patients. **g** The heatmap shows the DEGs of T cells among the HAs, herpes zoster patients (HP) and herpes zoster patients (RP) patients. **h**–**k** Blood routine analysis of the numbers and frequencies of monocytes and lymphocyte from HA and herpes zoster patients. Unpaired t-test were used and the data represent the means ± SEM. ***$P < 0.001$, ****$P < 0.0001$.

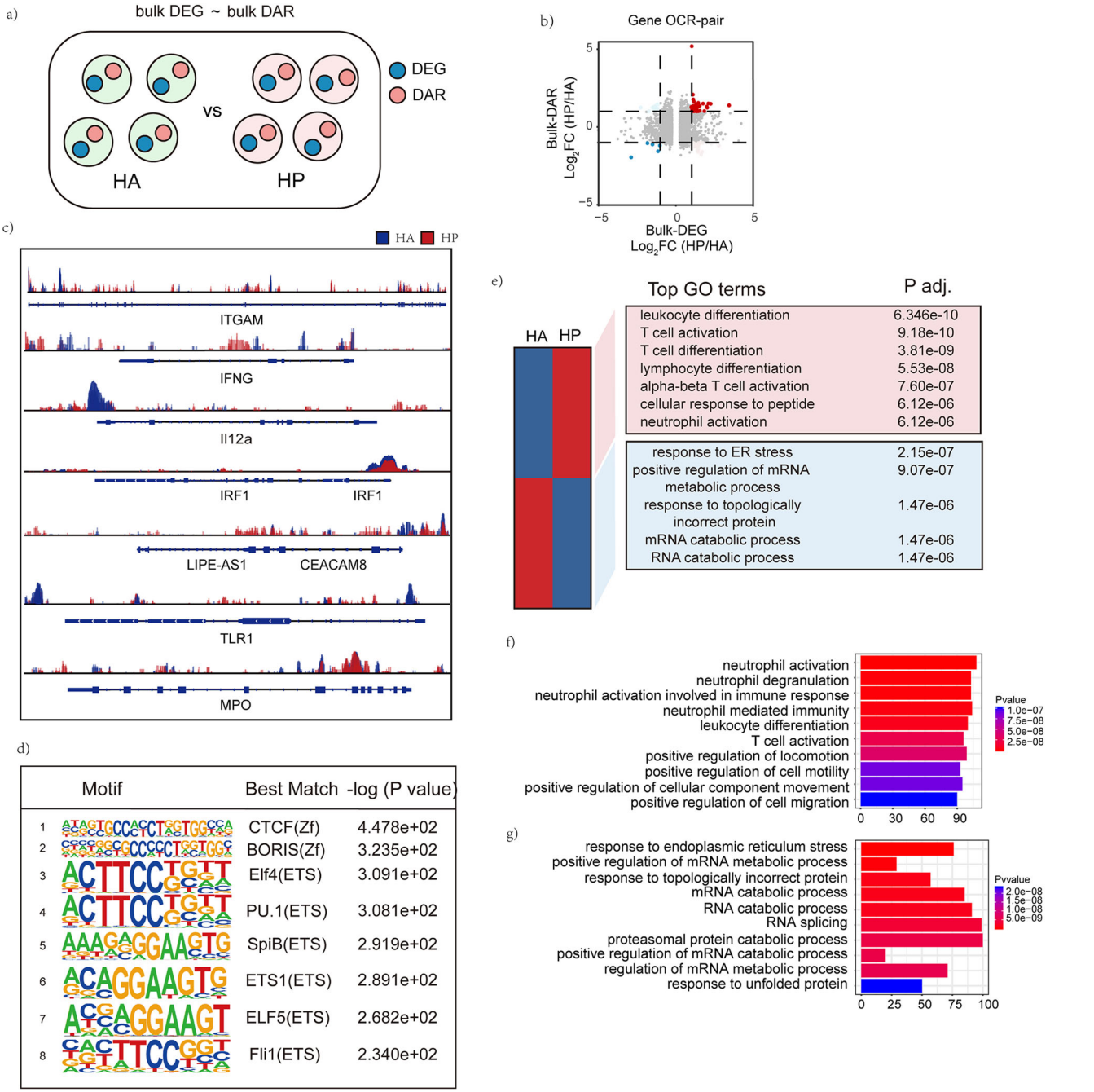

Fig. 3 | Integrated analysis of scRNA seq and ATAC-seq at bulk level. a Strategy to integrated analysis DEGs and DARs at bulk level. **b** Gene-OCR pairs determined by log2(fold change) of scRNA-seq and ATAC-seq at the bulk level. **c** The top 8 motifs motif analysis of the up-regulated Peaks and the predicted motif-related key transcription factors are shown. **d** Genome browser showing bulk-level ATAC-seq results for OCRs corresponding to key genes enriched in scRNA-seq analysis between HA and HP are displayed. **e** GO analysis of biological processes related to more open chromatin regions and less open chromatin regions. KEGG analysis of biological processes related to **f** more open chromatin regions and **g** less open chromatin regions.

Furthermore, a significant difference was found between HA, HP and RP (Fig. 5m). The cells from HA group were mainly concentrated in state1, while the HP and RP group were primarily enriched in state2 and state3. The distribution was slightly different in two group, predominantly showed in proliferating T cells and NK Cells. Considering the function of memory T cells associated with viral infection, we designed a gating strategy to obtain CD8+Tem cells and CD8+ T effector cells (Fig. 5o). In both cases, the scRNA-seq findings were directly validated using cytometric data (Fig. 5p, q).

Neutrophil subpopulations and their status in the blood of patients with herpes zoster

In total, 25,859 neutrophils were retained and annotated into 5 subpopulations that were remodeled during herpes zoster progression (Fig. 6a–c). We identified 16 signature genes including *GNGT2, SOX4, RPL12, ELANE, PRTN3, MPO, TUBA1B, LTF, CAMP, MMP8, CXCL2, ISG15, RSAD2, IFIT3, FGL2 and GM2A* that distinguished each subpopulation (Fig. 6f). There was substantial differential gene expression between the groups. We identified 1359 differentially expressed genes (DEGs) related to the

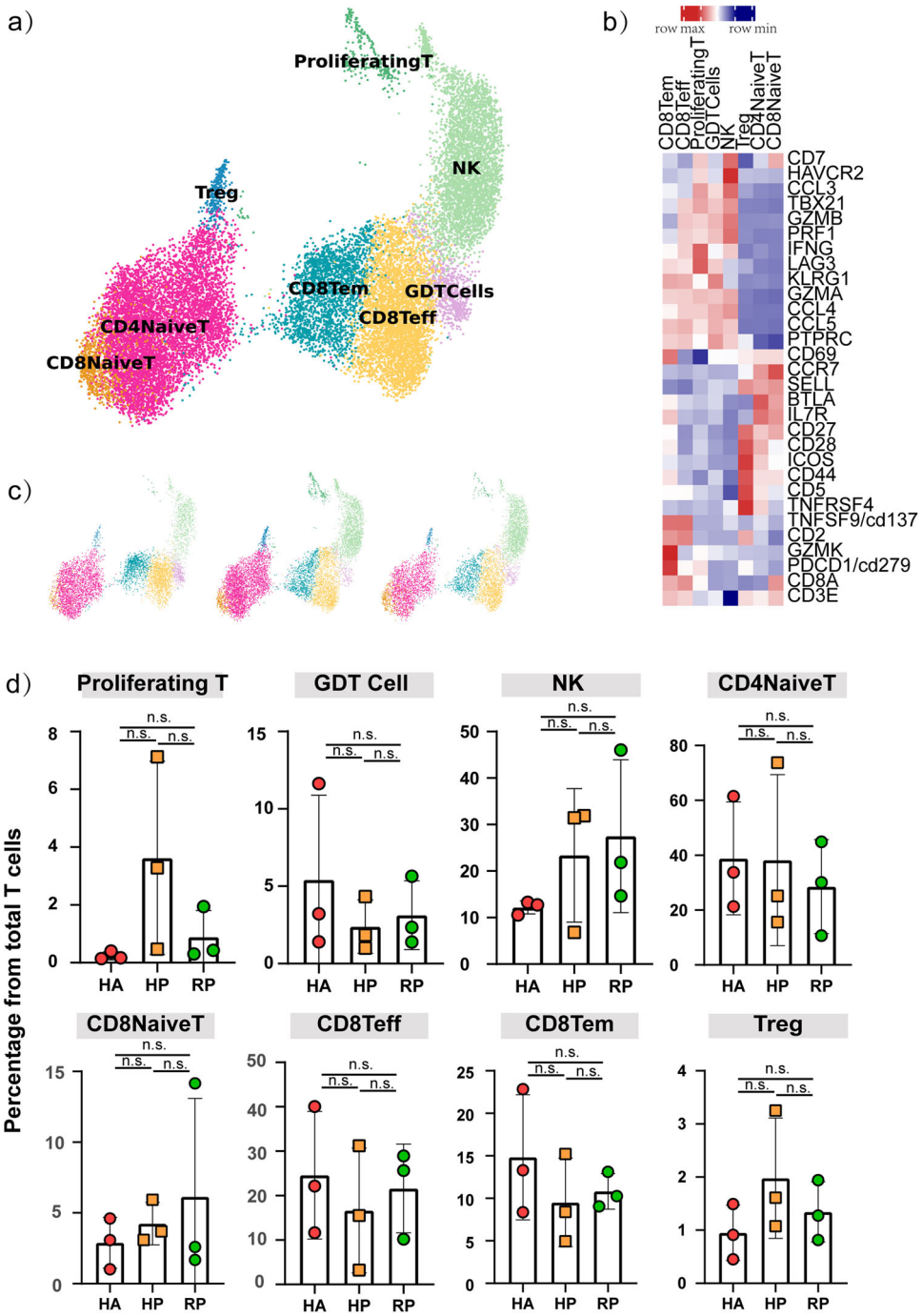

Fig. 4 | Characterization of T and NK cell states in the blood of patients with herpes zoster. a Three clusters of T and NK cell were displayed according to marker gene expression levels. Uniform manifold approximation and projection (UMAP) presentation of the heterogeneous clusters of T and NK cell, proliferating T cells, GDT cells, NK cell, CD4 naïve T cells, CD8 naïve T cells, CD8 Teff cells, CD8 Tem cells and Tregs. **b** Heatmap of subtype-specific marker genes of T and NK cell, including CD3E, CD8A, CD279, GZMK, CD2, CD137, TNFRSF4, CD5, CD44, ICOS, CD28, CD27, IL7R, BTLA, SEELL, CCR7, CD69, PTPRC, CCL5, CCL4, GZMA, KLRG1, LAG3, IFNG, PRF1, GZMB, TBX21, CCL3, HAVCR2 and CD7. **c** The UAMP plot shows the distribution of the eight subpopulations across HA, HP and RP group. **d** Box diagram of the relative frequencies of eight subpopulations across HA, HP and RP group.

regulation of immune responses, inflammatory factors, and cytokines that were significantly upregulated in the HP group (Fig. 6d).

In a gene ontology analysis of DEGs, the following processes were enriched in HP compared to HA: response to interleukin-1, positive regulation of neuron death, Ras protein signal transduction, macroautophagy, and cytoplasmic pattern recognition receptor signaling pathway, while defense response to virus, response to interferon−gamma, response to type I interferon, type I interferon signaling pathway, regulation of response to biotic stimulus, regulation of innate immune response were enriched in HA (Fig. 6e). To map the ligand-receptor interactions, we evaluated the potential cell-cell interactions between neutrophils and other cell subtypes by using CellPhoneDB, and demonstrated the top30 ligand-receptor interactions of neutrophils. Interestingly, the interactions between cells of the same type were stronger than those between different cell types. Neutrophils exhibited a tendency to communicate with MPs and platelets (Fig. 6g). Among the identified interactions, a significant number were associated with CXCL8 and its corresponding receptor CXCR1 (Fig. 6h). CXCL8 is not only a critical component of inflammation-mediated processes, but it has also been reported that neutrophil infiltration mediated by the CXCL8-CXCR1/2 axis occurs in neuro-inflammatory diseases[21,22]. We also detected a decreased neutrophil proportion in the HP group than HA group by flow cytometric analysis, which were consistent with scRNA-seq data (Fig. 6i, j). This suggests that neutrophils were highly involved in immune response.

Myeloid cell subpopulations and their status in the blood of patients with herpes zoster

To further understand the changes in Mononuclear phagocytes during different stages of herpes zoster, we conducted gene expression analysis and

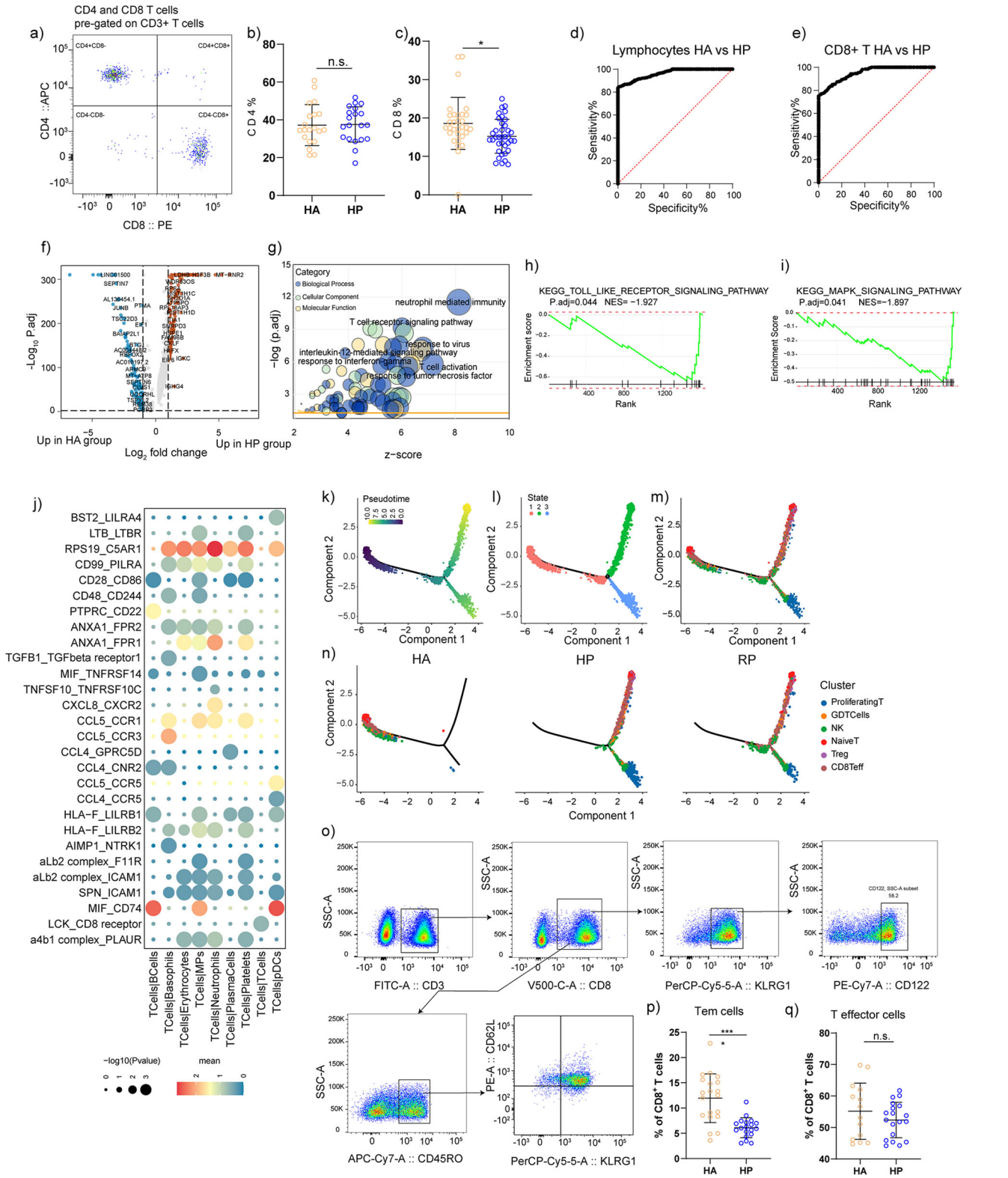

Fig. 5 | Validation for CD8+ T cell subpopulations. a Representative cytometric gating strategy for identification of T lymphocytes. **b** Proportion of peripheral CD4 T cell in HP and HA groups. **c** Proportion of peripheral CD8 T cell in HP and HA groups. **d** ROC curve for CD3+ T lymphocyte to separate hp from HA. AUC = 0.96. AUC, area under curve. **e** ROC curve for CD8+ T lymphocyte to separate hp from HA. AUC = 0.95. AUC, area under curve. **f** Volcano plot for comparison of HP vs. HA group in CD8 Teff cluster. **g** Bubble chart for GO enrichment analysis of the DEGs of CD8 Teff cluster upregulated in HP patients. *P* value was derived by a hypergeometric test. **h** GSEA plot for selected pathway positively enriched in CD8+ Teff cell cluster. **i** GSEA plot for selected signaling pathway positively enriched in CD8+ Teff cell cluster. **j** Heatmaps showing the top 30 cell–cell interactions in the scRNA-seq dataset of T cells, as inferred by CellPhoneDB. **k**–**m** Pseudotime trajectories to show the alignment of neutrophil subpopulations. Cells were colored by Pseudotime (**k**) subpopulation (**l**) or time (**m**). **o** Representative cytometric gating strategy for identification of CD8+ T lymphocytes. **p** Proportion of peripheral CD8 Tem cells in HP and HA groups. **q** Proportion of peripheral CD8 Teff cells in HP and HA groups.

sub-clustered the mononuclear phagocytes into three transcriptionally distinct subsets using Uniform Manifold Approximation and Projection (UMAP). Classical monocytes CD14++CD16−CD62L(SELL)+CCR2+ (ClassicalMono), Non-classical monocytes CD14+CD16+CXCR3+ (NonClassicalMono), and Conventional dendritic cells (cDCs) HLA-DR+ were present in the three distinct clusters (Fig. 7a, c). Overall, we found that the 3 subpopulations/clusters were altered among groups (Fig. 7b, d–f). In addition, these clusters were found to preferentially express signature genes (Fig. 7c). Not only the percent of the three clusters altered considerably, we found that the compartment of the monocyte subset differed remarkably among the HAs and patients (Fig. 7d–f).

240 differentially expressed genes (DEGs) between the HP and HA groups. Among these, 138 significantly upregulated including *CYBB, TLR4, TLR8, JAK2, CXCL10, HLA-A, IRF2* and 102 downregulated proteins (Student's *t* test, $P < 0.05$, and fold change >2 or <0.5) were detected in the HP group (Fig. 7g). We performed GO enrichment analysis and discovered that IL-1b signaling pathway, Toll-like signaling pathway and positive production of cytokines were significantly enriched in classical monocyte cluster, and ATP metabolic process, Fc receptor signaling pathway and IL-1b signaling pathway were enriched in nonclassical monocytes (Fig. 7i). Notably, IL1β expression values in a UMAP with simultaneous contrast indicated that IL1β was upregulated in the HP group and then decreased after recovery (Fig. 7h). We further investigated the enrichment analysis in RP group than HP group, it was noted that the pathways elevated in HP group compared with HA group was down-regulated in RP group than HP group, indicating that the pathways mentioned above functioned during the progression of herpes zoster and then return to normal levels after recovery shown in Supplementary Fig. 4.

For further validation, we compared the monocyte ratios between 10 patients and healthy individuals using flow cytometric analysis and observed that classical monocyte (CD14++ CD16−) were significantly upregulated in the patient group, while the proportion of nonclassical monocyte (CD14+ CD16++) counts was down-regulated (Fig. 7j–k). These results revealed that the elevated proportion of monocytes during the onset of herpes zoster secreted a large number of inflammatory signals, which was significantly different from that with HA group, and these signals might potentially serve as early signals to activate the immune system.

B cell clustering and status profiling in herpes zoster-bearing patients

We analyzed the distribution of B cells during the onset and recovery phases of herpes zoster. Our results categorized B cells into 3 sub-populations: Naive B cell expressing CD19, CD20 (MS4A1), IGHD, IGHM, IL4R, and TCL1A; plasma cells expressing high level of CD27, CD38 and IGHG1; and memory B cell expressing CD27, CD38, and IGHG (Fig. 8a, d).

The proportion of memory B cells was up-regulated in the HP group compared to the HA group, whereas the proportion returned to a normal level after recovery. The proportion of plasma cells were also highly elevated in the HP group compared to the HA group (Fig. 8b). DEG among the subpopulations of B cell had high expression levels of immune-related genes such as *IGKV4-1, CD79B, CD82, SCIMP, CLECL1, TCL1A*; chemokines, *CCR7*; and B cell signature genes, *ITGB1, IGHG1, IGHG4, IGHM, IL4R and TCL1A* (Fig. 8c). and inflammatory genes and inflammatory associated pathways were upregulated in HP group relative to that in the HCs (Fig. 8e, h).

Memory b-cells and plasma cells are important differentiated forms of b-cells that exercise immune functions. Go enrichment analysis showed that enriched genes of the memory B cell in the HP group were involved in antigen processing/ presentation-related pathways, and the B cell proliferation pathway; and DEGs in the plasma cells enriched IL-1 mediated signaling pathway, IL-12 mediated signaling pathway; Fc receptor signaling pathway and B cell activation (Fig. 8e). GSEA results indicated that the enrichment of KEGG_MAPK_SIGNALING_PATHWAY of memory B cells in HP group compared HA group, while an inverse enrichment was detected in the comparison of RP and HP group (Fig. 8f). Meanwhile, the enrichment of KEGG_OXIDATIVE_PHOSPHORYLATION was found in HP group than HA group, and an inverse enrichment was detected in RP compared with HP group[23,24] (Fig. 8g). We further explored the enrichment analysis in RP group than HP group, it was noted that the pathways elevated in HP group compared with HA group was down-regulated in RP group than HP group, indicating that the pathways mentioned above functioned during the herpes zoster progression and then returned to a normal level after recovery (Supplementary Fig. 5a–d). Meanwhile, the functional changes in memory B cells revealed that NIK/NF-kappa B signaling, stimulatory C-type lectin receptor signaling pathway, IL-12 mediated signaling pathway and Fc-gamma receptor signaling pathway were stimulated during the herpes zoster progression and maintained after recovery(Supplementary Fig. 5e–h).The elevated B cell proportion in the HP group than HA group were further validated by flow cytometric analysis using 18 patient samples and 19 control samples, which were consistent with scRNA-seq data (Fig. 8i, j). Taken together, our results highlight the accumulation of b cells in HP group and further pointing toward the potential functional significance of memory B cells and plasma cells.

Discussion

Herpes zoster is one of the most painful skin diseases, and approximately one-third of people will develop shingles in their lifetime[25,26]. Several studies have reported that adults diagnosed with COVID-19 may be more vulnerable to developing herpes zoster, which could further increase the burden on global health[27,28]. Despite the progress in treatment strategies, the incidence of herpes zoster remains high; functional status and health-related quality of life are severely compromised[29]. The painful rash and the accompanying long-term neuropathic pain suggest the urgent need for early diagnosis and rapid eradication based on a better understanding of the heterogeneity of the immune functioning system during the onset of herpes zoster[30]. Here we provide a comprehensive single-cell profile to characterize immune system in the onset of and recovery from herpes zoster.

The complexity of the immune populations profiled in our analysis was characterized by a higher proportion of T cells and MPs, and a lower proportion of B cells and neutrophils in the HP group.

T cell-mediated cellular immunity is essential for the control of herpes zoster infection[31–33]. Consistent with previous reports[34,35], We found that the proportion of CD8 Teff cells were decreased, while the enrichment analysis indicated the activation of CD8 Teff subpopulation in response to herpes zoster. Previous studies suggested the CD4+ T cell function on exposure to Varicella-Zoster Virus[36,37], the percentage of CD4+ T cells detected by flow cytometry in our study between HA group and HP group didn't reach statistical significance, and the ROC analysis suggested the AUC value of CD4+ T cells between HP and HA group was 0.5089. This may be caused by the functioning CD4+ T cell subpopulation compressed by the overall percentage of CD4+ T cells exhibited by flow cytometry without further breakdown of subpopulations. Monocyte exhibited to an inflammatory state in response to herpes zoster indicated by secretion of cytokines, such as IFN-gamma and IL1b, and inflammatory-associated pathways including the toll-like signaling pathway which was demonstrated to be critical in innate immune system activating anti-viral innate immune responses in host cells[38]. Previous study reported that B cell dysfunction increased the risk of herpes zoster infection[4]. Our study revealed that accumulated B cell subpopulation in response to herpes zoster and pointed toward the potential functional significance of memory B cells and plasma cells. In this study, the ratio of neutrophil was significantly decreased following herpes zoster infection, and the enrichment analysis highlighted the activation in response to herpes zoster infection.

The generalizability of the immune cell alterations detected by single-cell sequencing was also identified. First, we investigated the routine blood data for over 1000 patients with herpes zoster, in which the changes in lymphocytes and monocytes were consistent with the single-cell seq results. In addition, the distribution of subpopulations including CD8 Teff cells, CD8 Tem cells, classical monocytes, nonclassical monocytes B cells were

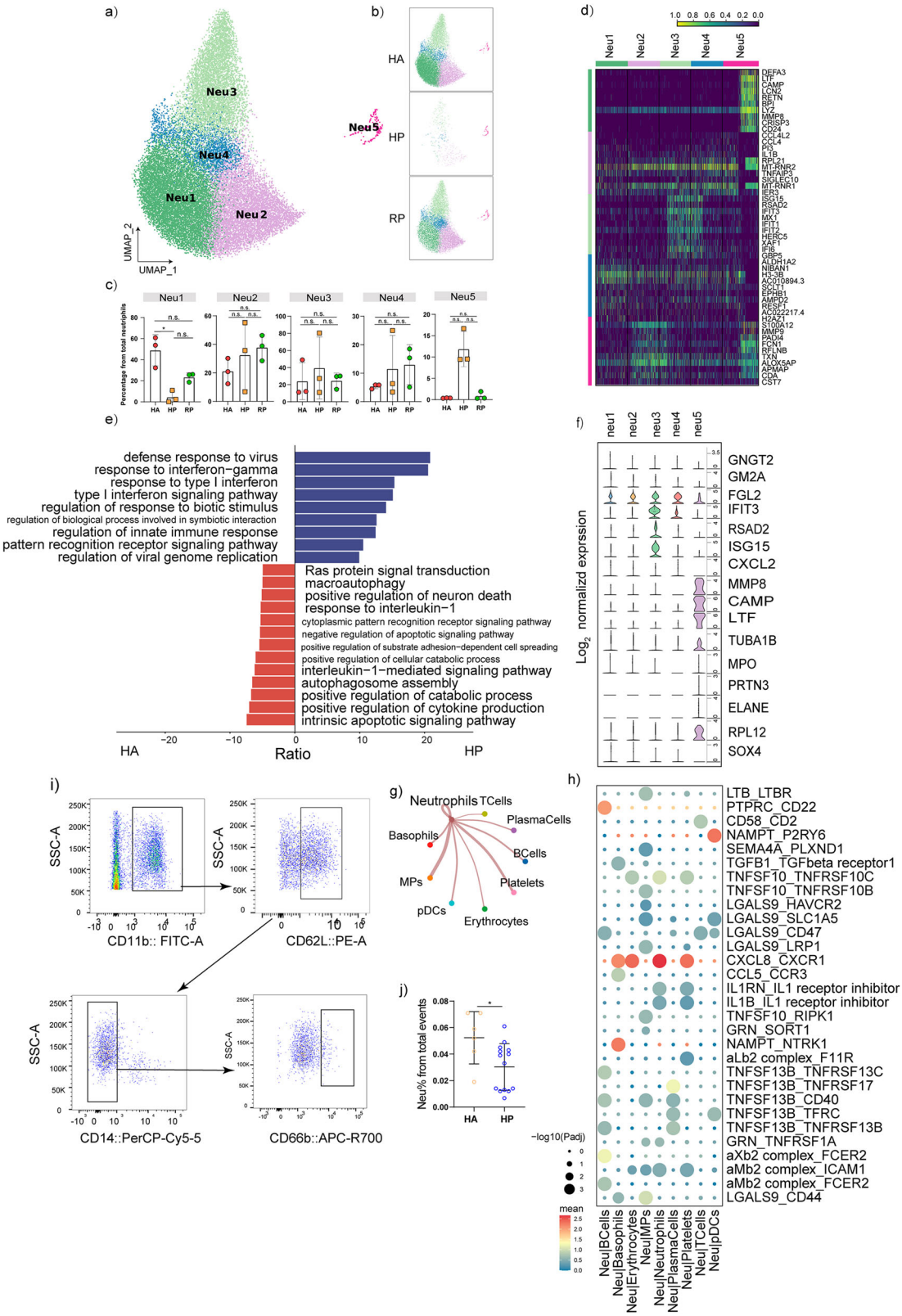

identified using flow cytometry containing over 90 samples, in which a consistent alteration with single cell-sequencing were also verified.

Our study represents an essential step toward understanding how the immune system responds to herpes zoster. The study of herpes virus latency and reactivation is a complex and actively researched topic within the scientific community. This is the first study to provide an elaborate single-cell profiling and validation of PBMCs during herpes zoster virus infection. Prior studies of the immune response during herpes virus infection usually focus on a specific type of immune cell, failing to provide a comprehensive immunological profile. By using single-cell sequencing, our analysis helps to understand the pathogenesis of herpes zoster, and provides inspiration for further clinical treatment strategies.

Fig. 6 | Characterization of neutrophils in patients with herpes zoster. a Five clusters of neutrophils were displayed according to marker gene expression levels. Uniform manifold approximation and projection (UMAP) presentation of the heterogeneous clusters of neutrophils. **b** The UAMP plot shows the distribution of the five subpopulations across HA, HP and RP group. **c** Box diagram of the relative frequencies of five subpopulations across HA, HP and RP group. **d** The heatmap shows the DEGs of five neutrophils subpopulations. **e** GO BP enrichment analysis for the DEGs of neutrophils in HP patients. The red terms represent upregulated terms, and the blue represent downregulated terms. *P* value was derived by a hypergeometric test. **f** Violin plot of subtype-specific marker genes of neutrophils, including GNGT2, GM2A, FGL2, IFIT3, RSAD2, ISG15, CXCL2, MMP8, CAMP, LTF, TUBA1B, MPO, PRTN3, ELANE, RPL12 and SOX4. **g** Network diagram of receptor-ligand interaction pairs between neutrophils and other cell types. Network nodes are cell types, network edge thickness is the total number of ligand-receptor pairs, and line color is consistent with ligand cell type. **h** Heatmaps showing the top 30 cell–cell interactions in the scRNA-seq dataset of T cells, as inferred by CellPhoneDB. **i** Representative cytometric gating strategy for identification of neutrophils. **j** Proportion of peripheral neutrophils in HP and HA groups.

Limitations

This study has several limitations. One intrinsic limitation of this study is the validation sampling in males mostly. We utilized two methods to validate the results of single-cell sequencing, including flow cytometric analysis (20 healthy vs. 19 patients) as well as an investigation of biochemical results (over 1000 samples). Due to the limitations of the sample size and the number of patients admitted to the hospital during the sample collection period for flow cytometric validation, make the balancing between men and women very challenging. Thus, our results refer to a mostly male adult population. But even with the available sample size we were able to reproduce previous results of the blood routine data which included both male and female patients (Fig. 2g–j), and identified a consistent immune cell alteration. Future in-depth studies require a much larger sample size, including sex and a much larger patient distribution.

Materials and methods

Human samples

Affiliated Hospital of Jiaxing University reviewed and approved this study for the collection of blood samples from healthy participants (LS2021-KY-024). Patients were diagnosed with herpes zoster at the Affiliated Hospital of Jiaxing University. Written informed consents were obtained from each participant. The 9 PBMC samples were collected from healthy controls, herpes zoster patients and recovered patients (Supplementary Table 1). The time point of blood collection in the hp group was at the patients' initial visit to the outpatient clinic, which was in the primary stage of confirming the diagnosis of herpes zoster. To serve as the RP group, the blood sample after recovery were collected 90 days after first negative diagnose date. Healthy controls did not have herpes zoster infection at or before the time of blood collection. No other differences were found for underlying diseases between the groups. For flow cytometric analysis, the blood samples collected ranged from ages 41–83 years old, with a median of 50 years old in the herpes zoster patients, a median of 46 years old in heathy controls (Supplementary Table 3). Blood collection for this study has been ongoing from 2021 to 2024.

RT & amplification & library construction

single-cell suspensions at a concentration of 2×10^5 cells/mL in PBS (HyClone) were loaded onto a microwell chip using the Singleron Matrix® Single Cell Processing System. Barcoding Beads were subsequently retrieved from the microwell chip, followed by reverse transcription of the mRNA captured by the Barcoding Beads to generate cDNA, and PCR amplification. The amplified cDNA was then fragmented and ligated with sequencing adapters. The single-cell RNA sequencing libraries were prepared following the protocol outlined in the GEXSCOPE® Single Cell RNA Library Kits (Singleron)[39].

Primary analysis of raw read data

Raw reads obtained from single-cell RNA sequencing (scRNA-seq) were analyzed using the CeleScope v1.9.0 pipeline (https://github.com/singleron-RD/CeleScope) to generate gene expression matrices. Initially, raw reads were processed with CeleScope to eliminate low-quality reads, trim poly-A tails, and remove adapter sequences using Cutadapt v1.17[40]. Cell barcodes and unique molecular identifiers (UMI) were then extracted. Subsequently, STAR v2.6.1a was utilized to align reads to the GRCh38 reference genome (Ensembl version 92 annotation)[41]. UMI counts and gene counts for each cell were obtained using feature Counts v2.0.1[42,43].

Quality control, dimension-reduction and clustering

Scanpy version 1.8.2 was utilized for conducting quality control, dimensionality reduction, and clustering analyses within the Python 3.7 environment[44]. Each sample dataset underwent filtration of the expression matrix based on specific criteria, including the exclusion of cells with a gene count of less than 200 or within the top 2% of gene count, cells with a top 2% UMI count, cells with mitochondrial content exceeding a specified threshold, and genes expressed in fewer than 5 cells. Following the filtration process, a total of 66338 cells were retained for subsequent analyses, with an average of 1052 genes and 2944 UMIs per cell. The raw count matrix was subsequently normalized by total counts.

Statistics and repeatability

Cell distribution comparisons between two groups were conducted using unpaired two-tailed Wilcoxon rank-sum tests, while comparisons of gene expression or gene signature between the two groups were performed using unpaired two-tailed Student's *t* tests. Additionally, comparisons of cell distribution within paired group 1 and group 2 were analyzed using paired two-tailed Wilcoxon rank-sum tests. The *p*-values used in this study were FDR-corrected. All statistical analyses and data presentation were carried out using the R software and python. The statistical tests utilized in the figures were detailed in the figure legends, and statistical significance was indicated.

Differentially expressed genes (DEGs) analysis

The analysis of differentially expressed genes (DEGs) was conducted using the Seurat FindMarkers function, which utilized a Wilcox likelihood-ratio test with default parameters. DEGs were identified as genes expressed in over 10% of cells within a cluster, with an average log (Fold Change) value exceeding 0.25. Cell type annotation for each cluster was achieved by integrating the expression of canonical markers identified within the DEGs, along with information from relevant literature sources. The expression patterns of markers for each cell type were visualized using heatmaps, dot plots, and violin plots.

Cell type annotation

The identification of cell type within each cluster was accomplished by assessing the expression of canonical markers present in the Differentially Expressed Genes (DEGs) using the SynEcoSys database. Heatmaps, dot plots, and violin plots illustrating the expression levels of these markers were generated using Seurat v3.1.2 DoHeatmap, DotPlot, and Vlnplot functions.

Pathway enrichment analysis

To examine the potential functions of Differentially Expressed Genes (DEGs), the study utilized Gene Ontology (GO) and Kyoto Encyclopedia of Genes and Genomes (KEGG) analysis with the "clusterProfiler" R package 3.16.1. Pathways with a p-adj value below 0.05 were deemed significantly enriched. Gene Ontology gene sets, encompassing molecular function (MF), biological process (BP), and cellular component (CC) categories, served as the reference. Gene Set Enrichment Analysis (GSEA) was conducted on a specified number of genes within distinct clusters. The GSVA pathway

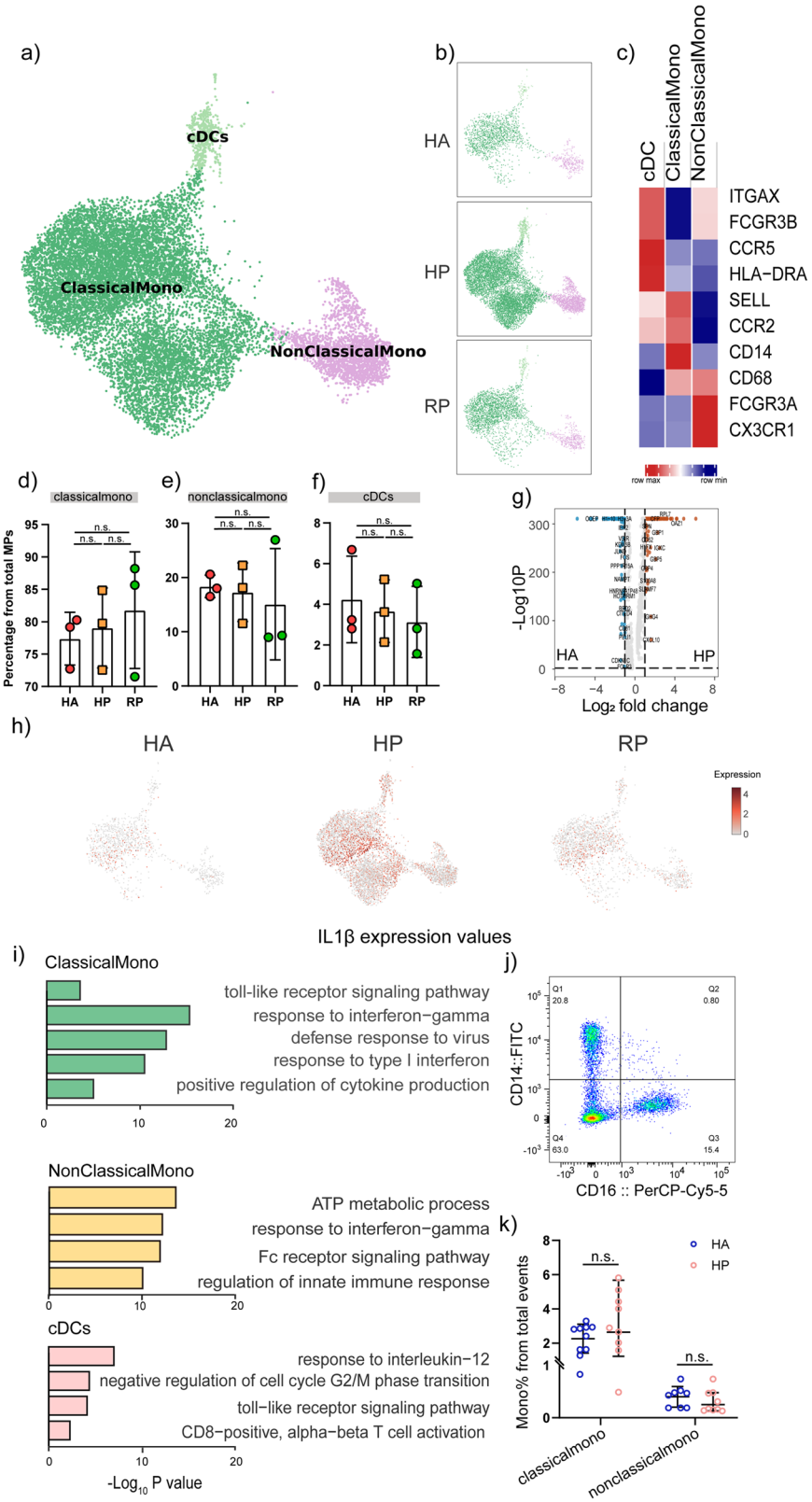

Fig. 7 | Myeloid cell subsets and their states in the blood of patients with herpes zoster. a Three clusters of myeloid cells were displayed according to marker gene expression levels. Uniform manifold approximation and projection (UMAP) presentation of the heterogeneous clusters of peripheral myeloid cells, Classical CD14++CD16− monocytes, non-classical CD14+CD16++ monocytes and cDCs. **b** The UAMP plot shows the distribution of the eight subpopulations across HA, HP and RP group. **c** Heatmap of subtype-specific marker genes of myeloid cells, including ITGAX, FCGR3B, CCR5, HLA-DRA, SELL, CCR2, CD14, CD68, FCGR3A and CX3CR1. **d** Box diagram of the relative frequencies of classical monocyte across HA, HP and RP group. **e** Box diagram of the relative frequencies of nonclassical monocyte across HA, HP and RP group. **f** Box diagram of the relative frequencies of cDCs across HA, HP and RP group. **g** Volcano plot for comparison of HP vs. HA group in classical monocyte cluster. **h** The UAMP plot shows that IL-1β was highly expressed in the HP patients compared with the RP patients and HCs in MPs. **i** GO BP enrichment analysis of the DEGs of the three subpopulations upregulated in HP patients. *P* value was derived by a hypergeometric test. **j** Representative cytometric gating strategy for identification of classical monocytes and nonclassical monocytes. **k** Proportion of peripheral classical monocytes and nonclassical monocytes in HP and HA groups.

enrichment analysis utilized the average gene expression of each cell type as input data through the GSVA package.

Trajectory analysis

Cell differentiation trajectory was reconstructed with Monocle2[45]. Highly-variable genes (HVGs) were used to sort cells in order of spatial-temporal differentiation. We used DDRTree to perform FindVairableFeatures and dimension-reduction. Finally, the trajectory was visualized by plot_cell_-trajectory function. Next, CytoTRACE[46] (a computational method that predicts the differentiation state of cells from single-cell RNA-sequencing data using gene Counts and Expression) was used to predict the differentiation potential of monocyte subpopulations.

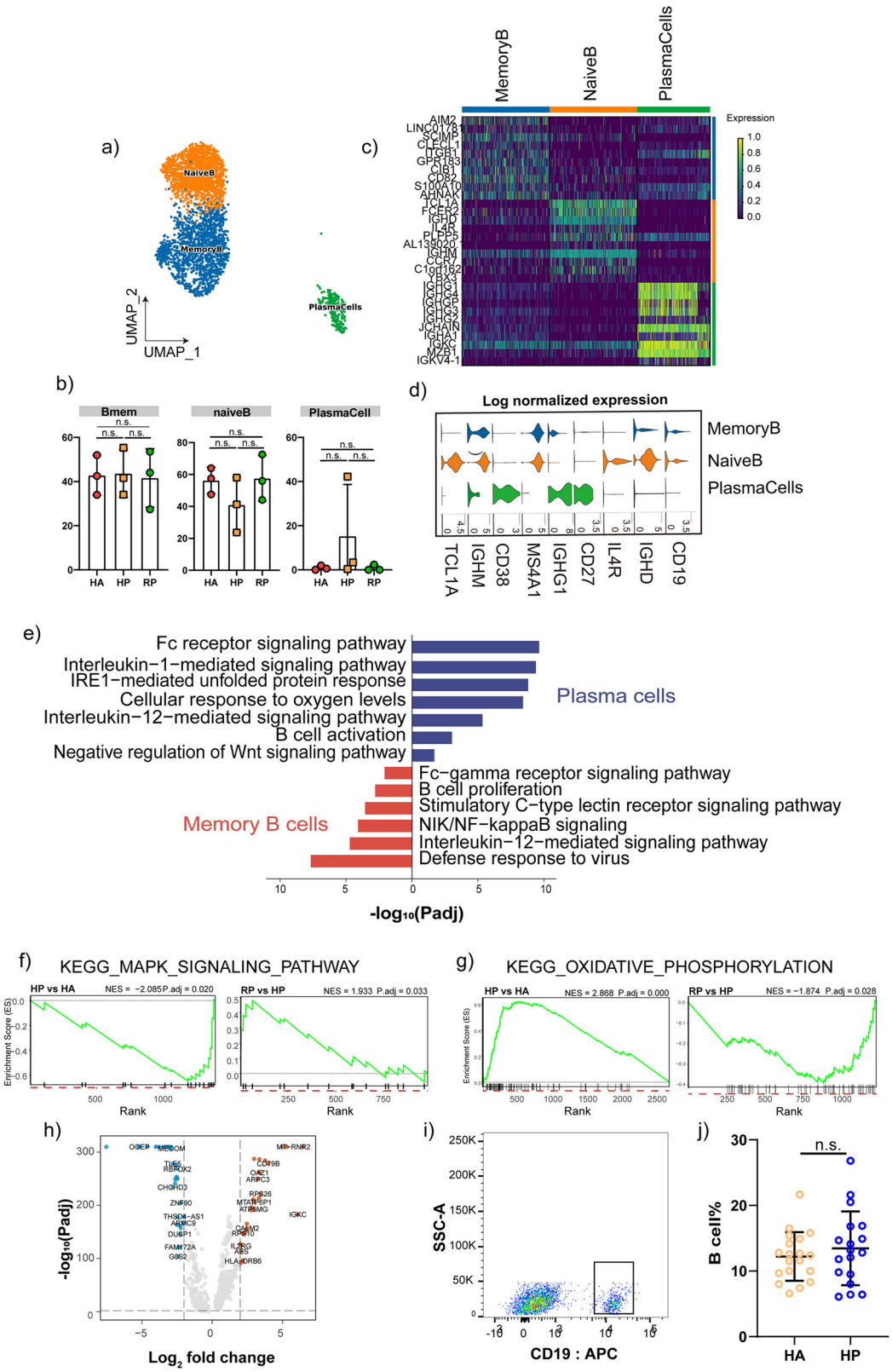

Fig. 8 | Characterization of B cells in patients with herpes zoster. a Three clusters of b cells were displayed according to marker gene expression levels. Uniform manifold approximation and projection (UMAP) presentation of the heterogeneous clusters of peripheral b cells, memory b cells, naïve b cells and plasma cells. **b** The bar plot shows the relative contributions of three subpopulations by samples, including the HA, HP and RP group. **c** The heatmap shows the DEGs of b cells between the HAs and herpes zoster patients (HP). **d** violin plot of subtype-specific marker genes of b cells, including CD19, IGHD, IL4R, CD27, IGHG1, MS4A1, CD38, IGHM and TCL1A. **e** GO BP enrichment analysis for the DEGs of memory b cell and plasma cells upregulated in HP patients. *P* value was derived by a hypergeometric test. **f** GSEA plot for selected pathway positively enriched in b cell cluster. **g** GSEA plot for selected signaling pathway positively enriched in b cell cluster. **h** Volcano plot for comparison of HP vs. HA group in b cell cluster. **i** Representative cytometric gating strategy for identification of b cells. **j** Proportion of peripheral b cells in HP and HA groups.

Cell-cell interaction analysis

The cell-cell interaction analysis was performed by CellPhoneDB v2.1.0[47] based on known receptor–ligand interactions between two cell types/subtypes. Cluster labels of all cells were randomly permuted for 1000 times to calculate the null distribution of average ligand-receptor expression levels of the interacting clusters. Individual ligand or receptor expression was thresholded with a cutoff value based on the average log gene expression distribution for all genes across all the cell types. The significant cell-cell interactions were defined as p value < 0.05 and average log expression >0.1, which were visualized with the circlize v0.4.10 R package.

ATAC-seq library construction and sequencing

Cell harvest and count cells. After the cells were counted, 50,000 cells were pretreated with DNase for 30 min at 37 °C to remove free-floating DNA and to digest DNA from dead cells. Cells were centrifuged at 500r.c.f. for 5 min. After centrifugation, resuspend the cell pellet in 50ul cold lysis buffer. This cell lysis reaction was incubated on ice for 3 min. After lysis, 1 ml of ATAC-seq RSB was added, Nuclei were then centrifuged for 10 min at 500r.c.f. After centrifugation,Nuclei were resuspended in 50 µl of transposition mix (10 µl 5×TD buffer, 5 µl Tn5 transposase,35 µl water).Transposition reactions were incubated at 37 °C for 30 min in a thermomixer with shaking at 1000 r.p.m. Reactions were cleaned up with Zymo DNA Clean and Concentrator 5 columns. PCR and size selection. DNA were resuspended in 25 µL of 2× HiFi PCR mix, 1 µL of each Nextera i5 primer (N5xx) and Nextera i7 primer (N7xx).The following PCR program was performed: 72 °C for 5 min, 98 °C for 1 min, 14 cycles at 98 °C for 15 s, 60 °C for 30 s, and 72 °C for 1 min. After PCR, Size selection with the DNA Clean Beads, 35 µL of DNA Clean Beads were added, Supernatant was transferred to a new tube, and 10 µL of fresh beads was added to capture fragments range from 250 to 350 bp. Libraries were quantified with Bioptic Qsep100 Analyzer (Bioptic link.), and paired-end sequenced with read lengths of 150.

ATAC-seq data processing

The ENCODE ATAC-seq pipeline was used for quality control and statistical signal processing of short-read sequencing data, producing alignments and measures of enrichment. 150 bp paired-end reads were mapped to the reference genome build (human, hg38; mouse, mm10). Differentially sites were detected from ATAC-seq experiments using DiffBind R package.

Comparison analysis between DEGs and DARs

The DEGs and ATAC differential peaks associated with genes were merged by gene symbol, and a four-quadrant plot was drawn based on the mRNA and ATAC differential ploidy, with a screening threshold of (mRNA: absolute value of differential ploidy is greater than 1, and p-value is less than 0.05; ATAC: absolute value of differential ploidy is greater than 1, and p-value is less than 0.05) labeled with an orange point. Note: Differential logFC0 results are also provided without differential ploidy screening, at which time the screening thresholds are (mRNA: p-value less than 0.05; ATAC: p-value less than 0.05) marked as orange points.

PBMC isolation

The whole blood underwent PBMC isolation through density gradient centrifugation using Histopaque-1077 in accordance with the manufacturer's guidelines. Specifically, the blood was mixed in a 1:1 ratio with D-PBS (Absin, abs970) containing 2 mM EDTA(Corning, 46-034-CI), the diluted blood were overlaid on Lymphocytes separation medium(Absin, abs930), and centrifuged at 2000 rpm for 30 min at 4 °C. PBMC were then extracted from the plasma-Histopaque interface. After washed in D-PBS(Absin, abs970) with 2 mM EDTA(Corning, 46-034-CI), extracted PBMCs were cryopreserved in Cell freezing solution(Absin, abs9417), and stored at −80 °C.

Flow cytometry

Cryopreserved PBMC were thawed and suspended with PBS containing 2% FBS (Gibco, SV30208.02). The surface antibody cocktail (details of antibodies shown in Supplementary Table 2, and the panel information were shown in Supplementary Table 3) was directly added to the cells and incubated for an additional 30 minutes at 4 °C. Flow cytometry data were acquired using FACSCanto II (BD Biosciences) instrument equipped with 2 lasers. results were then analyzed using FlowJo v10.6 software (Tree Star).

Quantification and statistical analysis

Data analysis was conducted utilizing the GraphPad Prism 9 software suite (GraphPad Software, San Diego, CA, USA). Experimental data were derived from three independent biological replicates. Statistical tests between three or more groups were performed with one-way ANOVA and between two groups were performed using Student's t test, with a threshold for statistical significance set at $p < 0.05$.

Reporting summary

Further information on research design is available in the Nature Portfolio Reporting Summary linked to this article.

Data availability

All data are available in the main text, Methods, Supplementary Information or Supplementary Data. Numerical source data for figures in the manuscript can be found in Supplementary Data 1-2. The raw sequence data reported in this paper have been deposited in the Genome Sequence Archive (Genomics, Proteomics & Bioinformatics 2021) in National Genomics Data Center (Nucleic Acids Res 2022), China National Center for Bioinformation / Beijing Institute of Genomics, Chinese Academy of Sciences (GSA-Human: HRA008316) that are publicly accessible at https://ngdc.cncb.ac.cn/gsa-human [48,49].

Code availability

This article contains no original code. The codes used in this article are shown in https://github.com/zhengshang1300/Single-cell-immune-profiling-and-validation-of-PBMCs-in-the-onset-of-and-recovery-from-herpes-zoster.

Received: 8 April 2024; Accepted: 18 November 2024;
Published online: 04 December 2024

References

1. Cohen, E. J. & Jeng, B. H. Herpes Zoster: A Brief Definitive Review. *Cornea* **40**, 943–949 (2021).
2. Harpaz, R., Leung, J. W. The Epidemiology of Herpes Zoster in the United States During the Era of Varicella and Herpes Zoster Vaccines: Changing Patterns Among Older Adults. *Clin. Infect. Dis.*, https://doi.org/10.1093/cid/ciy953/5213085 (2018).
3. Rafael Harpaz, J. W. L. The Epidemiology of Herpes Zoster in the United States During the Era of Varicella and Herpes Zoster Vaccines: Changing Patterns Among Children. *Clin. Infect. Dis.*, https://doi.org/10.1093/cid/ciy954/5213086 (2018).
4. Chen, M.-H. et al. Risk of depressive disorder among patients with herpes zoster: a nationwide population-based prospective study. *Psychosom. Med.* **76**, 285–291 (2014).
5. Jeon, Y. H. Herpes Zoster and Postherpetic Neuralgia: Practical Consideration for Prevention and Treatment. *Korean J. Pain.* **28**, 177–184 (2015).
6. Kennedy, P. G. In *Infections of the nervous system*, 177–208 (Elsevier, 1987).
7. Gershon, A. A. et al. Varicella zoster virus infection. *Nat. Rev. Dis. Primers.* **1**, 1–18 (2015).
8. Seixas, R., Dias, F., Ribeiro, A., Sobral, S. & Rita, H. Herpes Zoster Infection in an Immunocompromised Patient: A Case Report and Review of Corticosteroid's Role. *Cureus*, https://doi.org/10.7759/cureus.20908 (2022).
9. Johnson, R. W. et al. The impact of herpes zoster and post-herpetic neuralgia on quality-of-life. *BMC Med.* **8**, 37 (2010).

10. Chen, S.-Y. et al. Incidence of herpes zoster in patients with altered immune function. *Infection* **42**, 325–334 (2014).
11. Blennow, O. et al. Varicella-zoster reactivation after allogeneic stem cell transplantation without routine prophylaxis? the incidence remains high. *Biol. Blood Marrow Transpl.* **20**, 1646–1649 (2014).
12. Kawai, K., Gebremeskel, B. G. & Acosta, C. J. J. B. O. Systematic review of incidence and complications of herpes zoster: towards a global perspective. *BMJ Open* **4**, e004833 (2014).
13. Sly, J. R. & Harris, A. L. Recombinant Zoster Vaccine (Shingrix) to Prevent Herpes Zoster. *Nurs. Womens Health* **22**, 417–422 (2018).
14. Wei, L. et al. Decreased absolute numbers of CD3+ T cells and CD8+ T cells during aging in herpes zoster patients. *Sci. Rep.* **7**, https://doi.org/10.1038/s41598-017-15390-w (2017).
15. Tsukahara, T., Yaguchi, A. & Horiuchi, Y. Significance of monocytosis in varicella and herpes zoster. *J. Dermatol.* **19**, 94–98 (1992).
16. Gerada, C. et al. Manipulation of the Innate Immune Response by Varicella Zoster Virus. *Front. Immunol.* **11**, https://doi.org/10.3389/fimmu.2020.00001 (2020).
17. David, S., Richard, F., George, J. & Thomas, M. Cellular Events in Zoster Vesicles: Relation to Clinical Course and Immune Parameters. *J. Infect. Dis.* **131**(5), 509–515 (1975).
18. Sim, J.-H. et al. Association between Neutrophil-Lymphocyte Ratio and Herpes Zoster Infection in 1688 Living Donor Liver Transplantation Recipients at a Large Single Center. *Biomedicines* **9**, https://doi.org/10.3390/biomedicines9080963 (2021).
19. Liu, P., Zhang, M., Zhang, Y., Yu, S. & Wu, R. Neutrophil-lymphocyte ratio: an independent predictor of the herpes zoster risk in rheumatoid arthritis patients treated with tofacitinib. Aktuelle Rheumatologie. (2024).
20. Yamamoto, T. Roles of the ribosomal protein S19 dimer and the C5a receptor in pathophysiological functions of phagocytic leukocytes. *Pathol. Int.* **57**, 1–11 (2006).
21. Kimura, A. et al. Longitudinal analysis of cytokines and chemokines in the cerebrospinal fluid of a patient with neuro-Sweet disease presenting with recurrent encephalomeningitis. *Intern. Med.* **47**, 135–141 (2008).
22. Ha, H., Debnath, B. & Neamati, N. Role of the CXCL8-CXCR1/2 axis in cancer and inflammatory diseases. *Theranostics* **7**, 1543 (2017).
23. Hodes, R. J., Hathcock, K. S. & Weng, N.-P. J. N. R. I. Telomeres in T and B cells. *Nat. Rev. Immunol.* **2**, 699–706 (2002).
24. Chen, J. et al. Lis1 Regulates Germinal Center B Cell Antigen Acquisition and Affinity Maturation. *J. Immunol.* **198**, 4304–4311 (2017).
25. Albrecht, M. A., Levin, M. J., Hirsch, M. & Mitty, J. Epidemiology, clinical manifestations, and diagnosis of herpes zoster. UpToDate. Waltham, MA: UpToDate. (2020).
26. Shiraki, K., Toyama, N., Daikoku, T. & Yajima, M. Herpes Zoster and Recurrent Herpes Zoster. *Open Forum Infect. Dis.* **4**, https://doi.org/10.1093/ofid/ofx007 (2017).
27. Bhavsar, A. et al. Increased Risk of Herpes Zoster in Adults ≥50 Years Old Diagnosed With COVID-19 in the United States. *Open Forum Infect. Dis.* **9**, https://doi.org/10.1093/ofid/ofac118 (2022).
28. Diez-Domingo, J. et al. Can COVID-19 Increase the Risk of Herpes Zoster? A Narrative Review. *Dermatol. Ther.* **11**, 1119–1126 (2021).
29. Schmader, K. Herpes Zoster. *Ann. Internal Med.* **169**, https://doi.org/10.7326/aitc201808070 (2018).
30. Doneddu, P. E. et al. Neuropathic Pain in the Emergency Setting: Diagnosis and Management. *J. Clin. Med.* **12**, https://doi.org/10.3390/jcm12186028 (2023).
31. Feldman, S., Hughes, W. T. & Daniel, C. J. P. Varicella in children with cancer: Seventy-seven case. *Pediatrics* **56**, 388–397 (1975).
32. Seidlein, L. V. et al. Frequent recurrence and persistence varicella-zoster virus infections in children infected with human immunodeficiency virus type 1. *J. Pediatr.* **128**(1), 52–57 (1996).
33. Burchum, J., Rosenthal, L., Jones, B., Neumiller, J. & Lehn, R. J. M. E. S. *Lehne's pharmacology for nursing care*, 9th ed. (St Louis, 2016).
34. Weinberg, A., & Levin, M. J. VZV T cell-mediated immunity. Varicella-Zoster Virus, 341–357 (2010).
35. Steain, M. et al. Analysis of T Cell Responses during Active Varicella-Zoster Virus Reactivation in Human Ganglia. *J. Virol.* **88**, 2704–2716 (2014).
36. Vossen, M. T. et al. Development of virus-specific CD4+ T cells on reexposure to Varicella-Zoster virus. *J. Infect. Dis.* **190**, 72–82 (2004).
37. Park, H.-B. et al. Association of reduced CD4 T cell responses specific to varicella zoster virus with high incidence of herpes zoster in patients with systemic lupus erythematosus. *J. Rheumatol.* **31**, 2151–2155 (2004).
38. Zheng, W. et al. Toll-like receptor-mediated innate immunity against herpesviridae infection: a current perspective on viral infection signaling pathways. *Virol. J.* **17**, https://doi.org/10.1186/s12985-020-01463-2 (2020).
39. Dura, B. et al. scFTD-seq: freeze-thaw lysis based, portable approach toward highly distributed single-cell 3' mRNA profiling. *Nucleic Acids Res.* **47**, e16–e16 (2019).
40. Martin, M. Cutadapt removes adapter sequences from high-throughput sequencing reads. *EMBnet. journal* **17**, 10–12 (2011).
41. Dobin, A. et al. STAR: ultrafast universal RNA-seq aligner. *Bioinformatics* **29**, 15–21 (2013).
42. Liao, Y., Smyth, G. K. & Shi, W. an efficient general purpose program for assigning sequence reads to genomic features. *Bioinformatics* **30**, 923–930 (2014).
43. Townes, F. W., Hicks, S. C., Aryee, M. J. & Irizarry, R. A. Feature selection and dimension reduction for single-cell RNA-Seq based on a multinomial model. *Genome Biol.* **20**, 1–16 (2019).
44. Wolf, F. A., Angerer, P. & Theis, F. J. SCANPY: large-scale single-cell gene expression data analysis. *Genome Biol.* **19**, https://doi.org/10.1186/s13059-017-1382-0 (2018).
45. Qiu, X. et al. Single-cell mRNA quantification and differential analysis with Census. *Nat. Methods* **14**, 309–315 (2017).
46. Gulati, G. S. et al. Single-cell transcriptional diversity is a hallmark of developmental potential. *Science* **367**, 405–411 (2020).
47. Efremova, M., Vento-Tormo, M., Teichmann, S. A. & Vento-Tormo, R. CellPhoneDB: inferring cell–cell communication from combined expression of multi-subunit ligand–receptor complexes. *Nat. Protoc.* **15**, 1484–1506 (2020).
48. Xue, Y. et al. Database Resources of the National Genomics Data Center, China National Center for Bioinformation in 2022. *Nucleic Acids Res.* **50**, D27–D38 (2022).
49. Chen, T. et al. The Genome Sequence Archive Family: Toward Explosive Data Growth and Diverse Data Types. *Genomics Proteom. Bioinforma.* **19**, 578–583 (2021).

Acknowledgements

This study was supported by the Zhejiang Provincial Clinical Key Specialties-Anesthesiology (2023-ZJZK-001), and Jiaxing Key Laboratory of Neurology and Pain Medicine.

Author contributions

S.Z. and L.X. performed experiments and analyzed data; Y.F., K.S., Q.F. and S.Z. interpreted the results of experiments; Y.L., Q.Z. and B.L. prepared figures; S.Z drafted the manuscript; X.L. and M.Y. edited and revised the manuscript; L.X. conceived and designed the research. All authors approved the final version of the manuscript.

Competing interests

The authors declare no competing interests.

Additional information

Supplementary information The online version contains supplementary material available at https://doi.org/10.1038/s42003-024-07289-w.

Correspondence and requests for materials should be addressed to Ming Yao or Longsheng Xu.

Peer review information *Communications Biology* thanks the anonymous reviewers for their contribution to the peer review of this work. Primary Handling Editors: Shitao Li and Dario Ummarino. A peer review file is available.